Quantum oscillations in a lead chalcogenide three-dimensional Dirac system

Orbanić, Filip; Novak, Mario; Baćani, Mirko; Kokanović, Ivan

Repository / Repozitorij:

Repository of the Faculty of Science - University of Zagreb

☙

Quantum oscillations in a lead chalcogenide three-dimensional Dirac system

Filip Orbanić,[1] Mario Novak,[1,*] Mirko Baćani,[1,2] and Ivan Kokanović[1,3]

[1]*Department of Physics, Faculty of Science, University of Zagreb, 10002 Zagreb, Croatia*

[2]*Empa - Swiss Federal Laboratories for Materials Science and Technology, 8600 Dübendorf, Switzerland*

[3]*Cavendish Laboratory, University of Cambridge, Cambridge CB3 0HE, United Kingdom*

The de Haas–van Alphen (dHvA) and the Shubnikov–de Haas (SdH) oscillations were used to probe the properties of the Fermi surface in single crystals of $Pb_{0.83}Sn_{0.17}Se$ with reduced charge concentration. Pronounced low-frequency oscillations of $\sim$8 T in the [001] direction were observed, confirming the single Fermi surface cross section. Due to the low effective charge concentration, the ultraquantum limit is reached already at $\sim$10 T. We observe π-Berry phase shift in the phase of both dHvA and SdH oscillations, which confirms the 3D Dirac nature of the energy band dispersion. In the construction of the Landau level diagram we use a combined indexing method for conductivity, magnetic susceptibility, and magnetization, which is based on the indexing used in the topological insulators. Moreover, the reliability of the indexing method is increased because we use, beside minima and maxima, zeros of the oscillations as well. Different microscopic parameters were calculated from the quantum oscillations in the magnetization, conductivity, and resistivity.

I. INTRODUCTION

The lead-based chalcogenides are topological insulators (TIs) in which the time-inversion-symmetry protection of the Dirac point is replaced by the mirror crystal symmetry [1]. They are often referred to as the topological crystalline insulators (TCIs). By tuning the Sn concentration in $Pb_{1-x}Sn_xTe$ and $Pb_{1-x}Sn_xSe$, an ordinary insulator can be transformed to a TCI. Besides topologically protected surface states, the lead-based chalcogenides have an interesting low-temperature bulk energy dispersion, which is described by the massive 3D Dirac equation [2,3]. The bulk energy gap, i.e., the mass term of the 3D Dirac equation, depends on the Sn concentration. It is predicted that for $x = 0.35$ in $Pb_{1-x}Sn_xTe$ and $x = 0.17$ in $Pb_{1-x}Sn_xSe$ the energy gap is closed and consequently the system can be described by the massless 3D Dirac equation [4,5]. The 3D Dirac materials have drawn a lot of attention in the research community after the discovery of Cd_3As_2 and Na_3Bi, which are symmetry-protected 3D Dirac semimetals [6–10]. These materials are located at the phase transition between an ordinary insulator and a TI and, because of their linear energy dispersion, represent a 3D analog of graphene [11]. By breaking the time-inversion symmetry or the center-of-inversion symmetry, a 3D Dirac material can transform into a Weyl semimetal, a system where the Dirac cone is split into two spin-nondegenerated Weyl cones separated in reciprocal space [12,13]. The Weyl semimetals harbor several interesting phenomena such as the chiral anomaly, surface Fermi arc states, and the intrinsic anomalous Hall effect [14–17].

$Pb_{1-x}Sn_xTe$ and $Pb_{1-x}Sn_xSe$ have recently attracted much interest because of their topological surface states [5,18–22]. On the other hand, the 3D Dirac nature of its bulk energy dispersion has not been studied to a great extent. In this paper, we report on the thermodynamic de Haas–van Alphen (dHvA)

and the charge-transport Shubnikov–de Haas (SdH) quantum oscillations of a bulk 3D Dirac system $Pb_{0.83}Sn_{0.17}Se$ (PSS). This particular composition is selected in order to achieve the state of transition between the ordinary insulator and the TCI, where the existence of a zero band gap state is reported [5]. The dHvA oscillations were investigated with a dc superconducting quantum interference device (SQUID) magnetometer in a magnetic field up to $B = 5$ T and temperatures up to $T = 30$ K. The magnetization of PSS shows oscillations with $1/B$ periodicity and strong linear diamagnetism, the magnitude of which significantly exceeds the bare core magnetization. All the samples show single-frequency oscillations of the magnetization M in the frequency range 7.4 T to 8.7 T, along the [001] direction. Analysis of the oscillations reveals a phase shift which corresponds to the π-Berry phase and hence confirms the 3D Dirac nature of the energy dispersion. The transport measurements were preformed on the set of samples obtained by cleaving the samples used in the magnetization measurements. The samples were subjected to electrical transport measurements in magnetic fields up to $B = 15$ T. The resistivity ρ_{xx} shows strong SdH oscillations which reach the ultraquantum limit already at around 10 T, due to effective low charge concentration.

The phase analysis of the SdH oscillations in the conductivity channel σ_{xx} gives consistent result for all samples with the dHvA oscillations. However, the SdH resistivity oscillations give a misleading phase shift and incorrect total effective charge concentration for one of the samples which is due to an additional transport channel coming from the sample's inhomogeneity. This indicates the importance of analyzing also the conductivity and not just the resistivity in the case of the phase analysis. We also present a method for consistent indexing of the dHvA and the SdH oscillations and creating the Landau level diagram for the phase determination. The used indexing is common for topological insulators and the quantum Hall effect [23,24]. Finally, we calculated a series of parameters such as the Fermi velocity v_F, effective mass m_c, and Dingle temperature T_D.

---

*mnovak@phy.hr

II. EXPERIMENTAL

Single crystals of $Pb_{0.83}Sn_{0.17}Se$ were grown by a modified Bridgman method. A proper amount of high-purity elements was mixed in an evacuated double quartz tube ($<10^{-5}$ mbar) and melt at $1100\,°C$ for several days with frequent mixing to ensure homogeneity. The crystallization was carried out by a slow cooling down to $900\,°C$ with subsequent water quenching. The cubic (Fm-$3m$) crystal structure of the resulting material was confirmed by the powder x-ray diffraction. To obtain samples with the best characteristics, pieces of material were cut from a single-crystal ingot and isothermally annealed in Se vapors at various temperatures to reduce the number of Se vacancies and thus to reduce the number of charge carriers. In this paper we present the samples annealed at $435\,°C$, which have the lowest effective charge concentration. The initial effective charge concentration was determined by measurements of the Hall effect at room temperature. The samples were subjected to nuclear spectroscopy (proton scattering), which revealed that the desired composition of $Pb_{0.83}Sn_{0.17}Se$ was achieved.

The magnetization M was measured using a SQUID magnetometer (Quantum Design). The samples were fixed inside a long plastic straw that acted as a sample holder by inserting two pieces of additional straw. The absence of the inner pieces, or their overlap, in the sample region, over at most $±1$ mm, would give a T-independent offset in the magnetization data. For the samples' masses of 30–70 mg used here, $±1$ mm corresponds to a systematic shift of $±3 × 10^{-6}$ emu. The samples were first mounted and cooled in the SQUID magnetometer down to 5 K. Before starting a magnetic sweep the magnet was reset to reduce the remanent field effects. All intercepts at $B = 0$ T were $<1.6 × 10^{-5}$ emu for the measured crystals, and have been subtracted from the data reported here. M was measured along the [001] direction. Checks for possible ferromagnetic contamination were made by performing M vs B scans at 300 K, 110 K, and 30 K. No ferromagnetic contamination was found.

For the transport measurements, the electrical contacts in the six-point geometry were made by spot welding of a 25 μm platinum wire, which resulted in contact resistance on the order of 0.5 Ω. Resistivity and Hall measurements were carried out in a liquid-helium cryostat, using a constant-bias current (dc, 10 mA, i.e., typically $3 × 10^{-8}$ A/m^2) and a nanovoltmeter with a 10 GΩ input resistance up to 12 V of the signal. The magnetotransport measurements were carried out at stabilized temperature by performing a continuous scan from $+15$ T to -15 T, and vice versa. Using the position of the low-field minimum in the magnetoresistance an offset in the magnet driving current and the actual field was estimated to be <25 mT. During measurements, the transport current was in the [001] direction and the magnetic field perpendicular to it.

III. RESULTS AND DISCUSSION

Magnetization M of the two PSS samples with reduced charge concentration was measured at different T with B along the [001] direction. The two samples, A1 and B1, both had nominal 17% Sn concentration. They have elongated prismatic
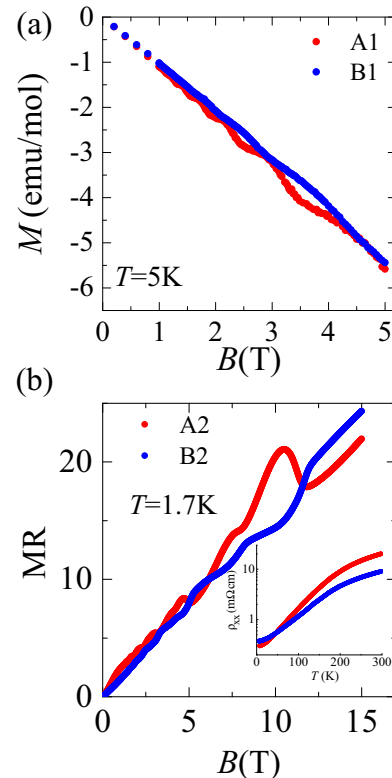

FIG. 1. (a) M of samples A1 and B1 at 5 K showing a linear dependence on B with the dHvA oscillations. In the case of the sample A1, the oscillations are considerably stronger in amplitude than for the sample B1. (b) Strong linear-like magnetoresistance $MR = [\rho_{xx}(B) - \rho_{xx}]/\rho_{xx}$ of samples A2 and B2 with pronounced SdH oscillations. For $B > 10$ T both samples are in the ultraquantum limit. The inset to Fig. 1(b) shows ρ_{xx} vs T for the samples A2 and B2.

shape with {001} terminating surfaces. Figure 1 shows $M(B)$ dependence (a) at $T = 5$ K up to $B = 5$ T and magnetoresistance (MR) (b) at 1.7 K up to 15 T. It can be seen from Fig. 1(a) that the magnetic response is diamagnetic, linear up to 5 T with notable dHvA oscillations. The diamagnetic response of $-1.10 × 10^{-4}$ emu/mol is stronger than the core diamagnetism of the constituent elements ($-7.46 × 10^{-5}$ emu/mol) of the sample. This is a very unusual result for an ordinary metal, but it is expected for materials such as Bi or narrow-gap semiconductors. In these materials, due to a very small effective electron mass and strong g factor, the Landau diamagnetic susceptibility becomes very large and strongly overcomes the Pauli paramagnetic susceptibility [4]. The dHvA oscillations are clearly visible starting from 1 T at 5 K, pointing to a low-frequency oscillation and high mobility in the samples. Several additional samples with slightly different annealing temperatures were measured and a similar behavior was observed.

The $MR = [\rho_{xx}(B) - \rho_{xx}]/\rho_{xx}$ measurements in the transverse orientation given in Fig. 1(b) reveal strong, linear-like, nonsaturating field dependence, reaching an increase of 2500% at 15 T and 1.7 K. The measured samples A2 and B2 were obtained by cleaving the magnetization samples A1 and B1, respectively. In spite of very strong linear MR background, the SdH oscillations are unusually pronounced and can be detected
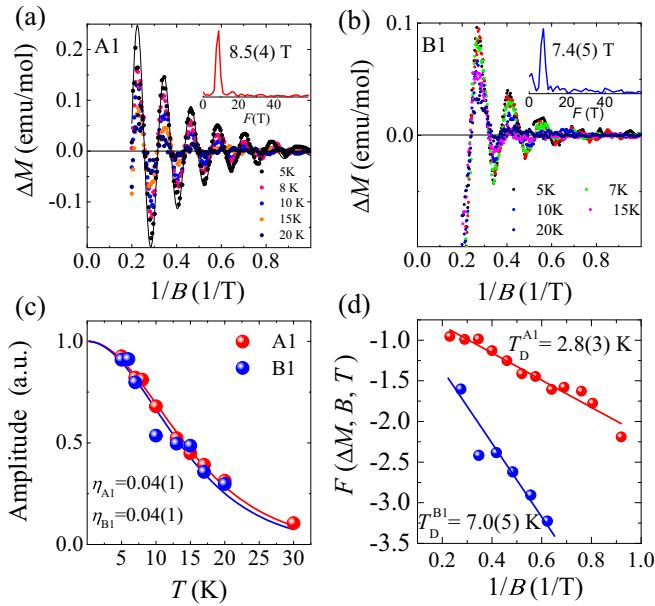
FIG. 2. Analysis of the oscillatory component of the magnetization ΔM for samples A1 and B1. Panels (a) and (b) show the temperature dependence of the dHvA oscillations. The oscillations start at a field as low as 1 T. In panel (a) Eq. (1) with fixed parameters [33] of F, m_c, T_D, and ϕ_p obtained by the indirect method as described in the text is fitted to the experimental data recorded at 5 K for sample A1. The inset shows the FFT analysis which reveals the single-frequency nature of the oscillations with $F_{FFT} = 8.5(4)$ T and $F_{FFT} = 7.4(5)$ T for samples A1 and B1, respectively. Using the LK theory the effective mass coefficient $\eta = m_c/m_e$ (c) and the Dingle temperature (T_D) (d) are obtained. (c) Temperature dependence of normalized oscillation amplitude for the peaks positioned at $B = 3.5$ T and 3.7 T, for samples A1 and B1, respectively, is used for retrieving the effective mass. The effective mass is $0.04(1)\,m_e$ for both samples, whereas sample B1 has a larger T_D, which is in accordance with a smaller oscillation amplitude for the sample B1. The vertical axis on panel (d) is $F(\Delta \rho_{xx}, B, T) = \ln(\Delta M B^{1/2} \sinh[2\pi^2 k_B T/\hbar\omega_c])$ with T set to 5 K.

from ∼1 T on at 1.7 K. The zero field resistivity shows the usual metallic-like temperature behavior with residual resistivities of $\rho_{1.7\,K}(A2) = 0.28\ m\,\Omega cm$ and $\rho_{1.7\,K}(B2) = 0.37\ m\,\Omega cm$ [see inset to Fig. 1(b)]. The origin of the strong linear MR is since recently a much debated question [25–30].

To extract the oscillatory part of magnetization ΔM, i.e., dHvA oscillations, we subtracted linear background from a strongly diamagnetic magnetization signal. Figures 2(a) and 2(b) show the dHvA oscillations for a set of temperatures in the range from 5–20 K for both samples. The oscillations are periodic in $1/B$, and the fast Fourier transform (FFT) analysis reveals single-frequency oscillations $F_{FFT}(A1) = 8.5(4)$ T and $F_{FFT}(B1) = 7.4(5)$ T; see the insets to Figs. 2(a) and 2(b). By increasing the temperature, the amplitude of the dHvA oscillations is reduced and for $T > 40$ K no traces of the oscillations could have been observed.

To extract useful information from the quantum oscillations we use the standard Lifshitz-Kosevich (LK) model for the 3D electron gas. Although the dHvA and SdH oscillations measure different physical quantities they can be represented by the

same functional form [31],

$$\Delta X(B,T) = A_0 A_T A_D A_S \left(\frac{B}{F}\right)^{1/2} \cos\left[2\pi\frac{F}{B} + \phi_p + \phi_M\right],$$

(1)

where ΔX stands for the oscillatory part of magnetization ΔM, magnetic susceptibility $\Delta\chi$, or conductivity $\Delta\sigma$ (resistivity $\Delta\rho$), A_0 is a dimensional constant, F the oscillation frequency, and ϕ_p the phase factor. $A_T = 2\pi^2(k_B T/\hbar\omega_c)/\sinh[2\pi^2(k_B T/\hbar\omega_c)]$, $A_D = \exp[-2\pi^2(k_B T_D/\hbar\omega_c)]$, and $A_S = \cos[\pi g m_e/(2m_c)]$ are the temperature, Dingle, and spin amplitude dimensionless prefactors, respectively. k_B is the Boltzmann constant, $\hbar$ the reduced Planck constant, g the Landé factor, $\omega_c = eB/m_c$ the cyclotron frequency, e the electron charge, and m_e free electron mass. ϕ_M is an additional phase factor, which discriminates between the SdH conductivity (resistivity), the dHvA susceptibility ($\phi_M = 0$), and the dHvA magnetization ($\phi_M = \pi/2$) oscillations. In the case of the 3D LK theory the amplitude prefactor of $\Delta X(B,T)$ bears an additional prefactor $(\frac{B}{F})^{1/2}$, which disappears in the 2D case [23,31,32]. The phase factor ϕ_p is defined as

$$\phi_p = 2\pi(\delta + \beta - 1/2),$$

(2)

where δ can change from 0 for a quasi-2D cylindrical Fermi surface (FS) to $\pm 1/8$ for a 3D FS, with (−) taken if the FS cross section is maximal and (+) if it is minimal. β is the Berry phase divided by 2π, taking values 0 for the Schrödinger and 1/2 for the Dirac electrons [23,31].

Analyzing the temperature dependence of the dHvA oscillation amplitudes at the peaks positioned at $B = 3.5$ T and 3.7 T, for samples A1 and B1, respectively, by using the LK formalism, we were able to extract the effective quasiparticle mass m_c, which gives a small effective mass of $m_c = 0.04(1)m_e$ for both samples. The Dingle temperature analysis was carried out at 5 K, and yields $T_D(A1) = 2.8(3)$ K and $T_D(B1) = 7.0(5)$ K, which points to a lower sample quality and stronger isotropic scattering in the case of the sample B1.

Figures 3(a) and 3(b) show the SdH oscillations in resistivity $\Delta\rho_{xx}$ for samples A2 and B2 extracted by removing a linear background from the measured signal. The oscillations are periodic in $1/B$. Above 10 T the system reaches the ultraquantum limit, which is also observed in Ref. [3]. The FFT taken for the low fields (below the spin splitting) gives the single-frequency peaks $F_{FFT}(A2) = 8.2(3)$ T and $F_{FFT}(B2) = 8.7(3)$ T. On the other hand, when the FFT is applied on the whole recorded interval we get additional peaks belonging to the higher harmonics emerging due to the spin splitting; see insets to Figs. 3(a) and 3(b). Since Eq. (1) does not pertain to a strong spin splitting case, in order to apply the LK formalism for extracting m_c and T_D we must restrict the analysis to the low-B region where the SdH oscillations do not show the spin splitting (single-frequency region). For both samples $m_c = 0.04(1)\,m_e$, which agrees with the dHvA data analysis. The analysis of T_D gives $T_D(A2) = 6.5(2)$ K and $T_D(B2) = 8.3(2)$ K, which are higher values than the corresponding ones obtained from the dHvA data analysis. The reason for this discrepancy is addressed later.

Another important physical quantity which we can extract from the dHvA and SdH oscillations is the phase of the
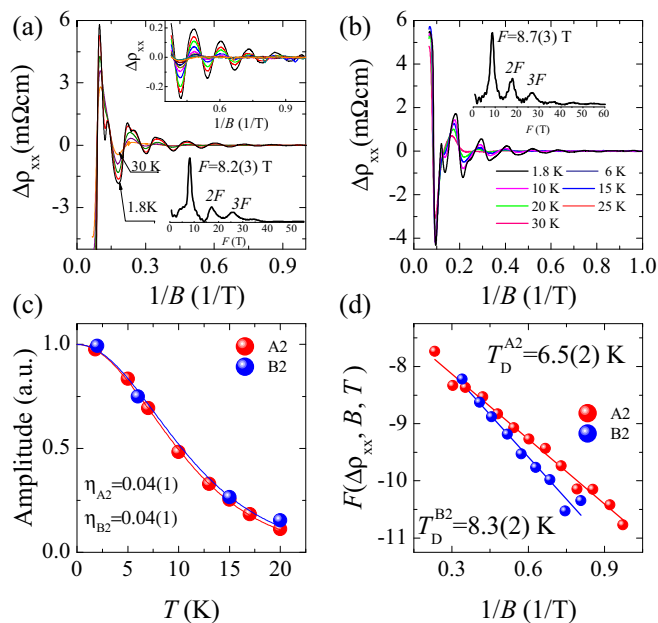
FIG. 3. Analysis of the SdH oscillations in resistivity $\Delta\rho_{xx}$, for the samples A2 (a) and B2 (b). Both panels shows the T dependence of the SdH oscillations after a linear background was subtracted. The peaks show the spin splitting at high magnetic fields. The inset shows the FFT analysis, which gives the peaks corresponding to the base frequency F and the higher harmonics ($2F$ and $3F$) that originate from the spin splitting. The LK analysis of T (c) and B (d) amplitude attenuation, for the fields where the spin split effects are neglectable, is used for retrieving m_c and T_D. The m_c values extracted from the amplitudes at $B = 2.38$ T and 2.5 T, for sample A2 and B2, respectively, agree with the effective mass obtained from the dHvA oscillations, whereas the SdH oscillations give a higher T_D than the dHvA oscillations. The vertical axis on panel (d) is $F(\Delta\rho_{xx},B,T) = \ln(\Delta\rho_{xx}B^{1/2}\sinh[2\pi^2 k_B T/\hbar\omega_c])$ with T set to 1.8 K.

oscillations. In order to combine the dHvA and SdH quantum oscillations in the same expression, we add an additional phase factor ϕ_M in Eq. (1) to distinguish between these two types of oscillations. From the phase of the oscillations we can resolve the Schrödinger (quadratic, $\beta = 0$) from the Dirac (linear, $\beta = 1/2$) dispersion. The term β in the case of band hybridization or mixing of the Dirac and Schrödinger term in the equation of motion can generally take any intermediate value between 0 and 1/2 [34,35]. Using the Landau level (LL) diagram, the phase factor ϕ_p, i.e, $(\delta + \beta)$ in Eq. (2), can be directly recovered from a plot as an intercept value on the horizontal axis. Here, we give a more universal method of indexing, which connects transport and magnetization data. To construct the LL indexing presented in Table I we used a method common for the topological insulators and in the integer quantum Hall effect [23]. In this method a minimum in σ_{xx} is associated with an integer N and a maximum with a half integer $N + 1/2$. Indexing for the magnetic quantities is derived according to the theoretical relation $\Delta\chi \sim \Delta\sigma_{xx}$, where $\Delta\chi$ is the oscillatory part of the magnetic susceptibility [31]. Notice the shift in indexing of minima in the magnetization for $-1/4$ in comparison to the minima in the magnetic susceptibility

TABLE I. LL indexing for conductivity σ, magnetic susceptibility $\chi = \partial M/\partial B$, and magnetization M. A minimum in $\Delta\sigma_{xx}$ was assigned to an integer N, and a maximum to a half integer $N + 1/2$. A zero crossing with the positive slope $0+$ is assigned to $N + 1/4$, whereas a zero crossing with the negative slope $0-$ to $N + 3/4$. Assignment of the magnetic oscillatory quantities is done according to the theoretical relation $\Delta\chi \sim \Delta\sigma_{xx}$, where $\Delta\chi$ is the oscillatory part of χ [31]. Using this method of indexing, depending on the FS shape, the horizontal axis intercepts 3/8 and 5/8 correspond to the 3D Dirac electrons and the intercepts of $-1/8$ and 1/8 to the 3D Schrödinger electrons. In the 2D case, as in the TI, the intercept of 1/2 corresponds to the Dirac electrons and 0 to the Schrödinger electrons. The presented indexing method produces overlapping curves with the same intercept for transport and magnetic quantities.

	$N - 1/4$	N	$N + 1/4$	$N + 1/2$	$N + 3/4$
$\Delta\sigma_{xx}$		min	0+	max	0−
$\Delta\chi$		min	0+	max	0−
ΔM	min	0+	max	0−	

and conductivity, which originates from the definition of the susceptibility $\chi = \partial M/\partial B$.

Figure 4(a) shows the indexing of the dHvA oscillations for samples A1 and B1. The indexing was done according to Table I, with minima, maxima, and zeros taken as the points for determining the horizontal axis intercept. The intercepts for samples A1 and B1 are $N_{A1} = 0.32(3)$ and $N_{B1} = 0.33(3)$, which is close to the theoretical value ($3/8 = 0.375$) predicted for the π-Berry phase shift. Taking the zeros into account in the indexing allows us a more precise determination of the intercept, i.e., the phase. This is especially important for the SdH oscillations since the high-B maxima have to be excluded from indexing due to the spin splitting. The F values can be independently retrieved from the slope of the indexing plot, which gives $F_{IN}(A1) = 8.4$ T and $F_{IN}(B1) = 7.2$ T. These values are consistent with the dHvA FFT results.

The next step was analyzing the SdH oscillations in ρ_{xx}; see Fig. 4(b). Due to the high B, the samples reach the ultraquantum limit, which allows us to make unambiguous LL indexing. However, it is puzzling why the indexing intercepts for the samples A2 and B2, in the case of SdH oscillations in ρ_{xx}, do not match. For the sample A2 the intercept is $N_{A2} = 0.5(3)$, suggesting the π-Berry phase shift, whereas for the sample B2 the intercept is $N_{B2} = -0.08(4)$, suggesting a trivial case, i.e., vanishing Berry phase. The dHvA oscillations observed in the sample from the same batch point to the π-Berry phase for both samples. To understand this discrepancy let us turn to the conductivity. In Fig. 4(c) the indexing was done on the basis of the SdH oscillations in the conductivity. The indexing of minima, maxima, and zeros was done as given in Table I, with minima in $\Delta\sigma_{xx}$ assigned with an integer N. In this indexing we count the number of filled LLs below the Fermi energy. For the sample A2 we get the intercept of $N_{A2} = 0.45(3)$ and from the slope we get the frequency of $F_{IN}(A2) = 8.2$ T, whereas for the sample B2 the intercept is $N_{B2} = 0.36(3)$ and the frequency $F_{IN}(B2) = 8.7$ T. The conductivity analysis proves that both samples have the π-Berry phase, as we expected. The frequencies from the index
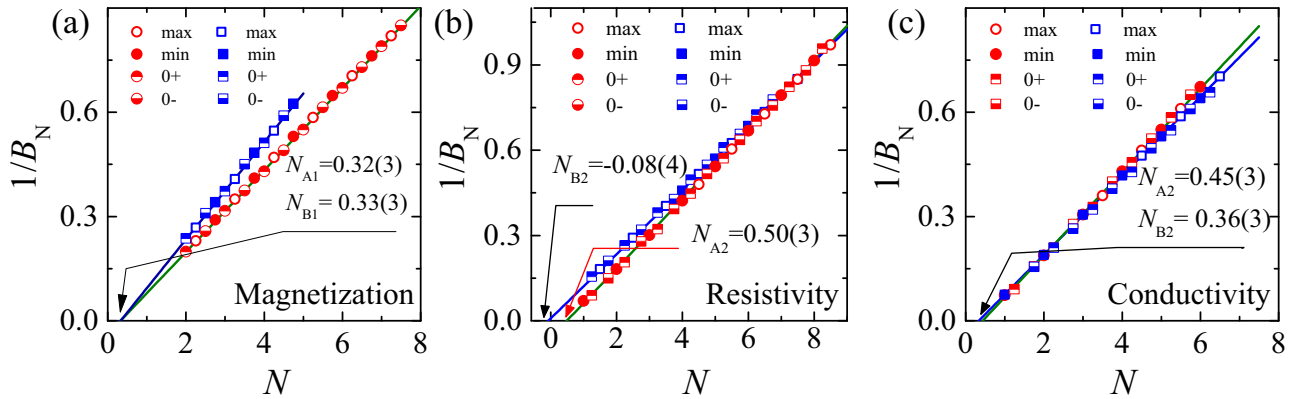
FIG. 4. LL diagrams for the oscillatory part of the magnetization ΔM, resistivity $\Delta\rho_{xx}$, and conductivity $\Delta\sigma_{xx}$. The intercept, indicated by an arrow, directly recovers the $(\delta + \beta)$ value from Eq. (2), and provides information on the Berry phase. For the Dirac case, $\beta = 1/2$, and $\beta = 0$ for the Schrödinger case, $\delta = \pm 1/8$. (a) Indexing of the dHvA magnetization data for samples A1 (red) and B1 (blue) gives the intercepts close to 3/8, which corresponds to the π-Berry phase shift. (b) The SdH resistivity indexing data. The intercept for the sample A2 (red) points to the existence of the π-Berry phase, whereas for the sample B2 (blue) it points to a vanishing Berry phase, which is in contradiction with the results obtained from the dHvA oscillations. (c) After transformation to the conductivity the intercepts of both samples, A2 (red) and B2 (blue), point to a π-Berry phase. For indexing of minima, maxima, and zeros for all three quantities we follow the rules given in Table I.

plot are contained within the error bars of the SdH FFT analysis given in Fig. 3.

The origin of the discrepancy in phase determination can be found in the definition of the SdH oscillations and the strength of the Hall signal. The symmetric tensor components of the conductivity are defined as $\sigma_{xx} = \rho_{xx}/(\rho_{xx}^2 + \rho_{yx}^2)$. Consequently, depending of the strength of the ρ_{yx}, oscillatory part of the conductivity $\Delta\sigma_{xx}$ can be in phase or out of phase with $\Delta\rho_{xx}$. For the sample A2, ρ_{yx} is stronger than ρ_{xx}, i.e., $\rho_{xx}(15\ \text{T}) = 0.067\ \Omega\,\text{cm}$ and $\rho_{yx}(1\ \text{T}) = 0.16\ \Omega\,\text{cm}$. On the other hand, for the sample B2 ρ_{yx} and ρ_{xx} are comparable, i.e., $\rho_{xx}(15\ \text{T}) = 0.092\ \Omega\,\text{cm}$ and $\rho_{yx}(15\ \text{T}) = 0.082\ \Omega\,\text{cm}$, which is the origin of the false phase determination from the resistivity.

Now we address the difference in T_D obtained from the dHvA and the SdH oscillations. We obtained $T_D(A1) = 2.8(2)\ \text{K}$ and $T_D(A2) = 6.5(2)\ \text{K}$. However, we expected comparable T_D in both samples since the temperatures at which the oscillations disappear are similar in both A1 and A2. Since it is strictly not satisfied $\rho_{yx} \gg \rho_{xx}$ as the theory demands, the amplitude prefactor is not as simple as given by Eq. (1). Thus, the dHvA oscillations in M give more reliable information on T_D. The same argument could be applied for the batch with B samples.

Finally, we calculate from the quantum oscillations additional useful parameters which characterize our system. The frequencies of the dHvA and SdH are related through the Onsager formula with the extremal area of the cross section of the FS in the plane normal to the external magnetic field [31]. In the case of circular FS cross section the Fermi wave vector k_F and F are related with $F = \hbar/(2\pi e)\pi k_F^2$. In the case of spherical FS, the total charge concentration per pocket located at the L point of the Brillouin zone can be estimated using the free electron gas model, $n_{3D} = k_F^3/3\pi^2$. At the same time, the charge concentration can be estimated from the Hall effect measurements. In the ideal case (single-band model) these two numbers should coincide. Here we shall focus on the

samples A2 and B2. If we make a comparison for the sample A2, we see that $n_{\text{SdH}}(A2) = 1.4 \times 10^{17}\ \text{cm}^{-3}$ and $n_H(A2) = 5.9(4) \times 10^{17}\ \text{cm}^{-3}$ are in good agreement (taking into account four electron pockets at the L point of the Brillouin zone). On the other hand, for the sample B2 this statement does not hold since $n_{\text{SdH}}(B2) = 1.4 \times 10^{17}\ \text{cm}^{-3}$ and $n_H(B2) = 11.6(5) \times 10^{17}\ \text{cm}^{-3}$. This implies the existence of an additional band, probably an impurity band, which provides additional charge carriers. This additional band contribution in the Hall effect is seen in the nonlinear dependence of ρ_{yx} vs B. The reduced Hall signal due to additional charge carriers is in turn responsible for obtaining a misleading Berry phase from the resistivity LL plot in the case of sample B2.

Furthermore, the dHvA oscillations in the sample B1 show notably different oscillation frequency than the SdH oscillations in the sample B2, which indicates not perfect sample homogeneity. Interestingly, the observed quantum oscillations in these samples are robust and not smeared out, which could be attributed to small m_c of the charge carriers and the low charge concentration in the system.

Knowing k_F and m_c allows us to calculate the Fermi velocity $v_F = \hbar k_F/m_c$. Here we focus on the sample A2, for which $v_F(A2) = 4.6 \times 10^5\ \text{m/s}$. This value of v_F is lower than in Cd_3As_2, where unusually high velocity is reported, and is in the range of velocities comparable to TIs [36,37]. The Fermi energy $E_F = \hbar v_F k_F$ is located 48 meV above the putative Dirac point. From T_D we obtain the quantum (isotropic) scattering time $\tau_q = \hbar/(2\pi k_B T_D) = 1.9 \times 10^{-13}\ \text{s}$, and the quantum mobility $\mu_q = e\tau_q/m_c = 7 \times 10^3\ \text{cm}^2/\text{V}\,\text{s}$. On the other hand, the Drude mobility is $\mu_t = 1/(en_H\rho_{1.8\,\text{K}}) = 3.8 \times 10^4\ \text{cm}^2/\text{V}\,\text{s}$, which combined with the Fermi velocity gives the mean-free path $l = 400\ \text{nm}$. The difference in the quantum and the Drude mobility originates in the different scattering mechanisms. In the Drude model the dominant scattering is the large-angle scattering whereas the quantum oscillations measure all scattering processes which are responsible for broadening of the LL, which also includes the forward scattering. The sample

B2 has lower τ_q, μ_q, and μ_t values indicating a lower sample quality in comparison to the sample A2.

IV. CONCLUSION

In conclusion, we have studied the de Haas–van Alphen (dHvA) and the Shubnikov–de Haas (SdH) oscillations as two complementary methods to probe the Fermi surface on two single crystals of $Pb_{0.83}Sn_{0.17}Se$. In our study, the dHvA and SdH oscillations reveal single frequency, of around 8 T along the [001] direction, which confirms the existence of a single Fermi surface cross section. Both the transport (SdH) and magnetic (dHvA) measurements support a nontrivial π-Berry phase shift with the intercept close to 3/8, which is evidence of the existence of the 3D Dirac dispersion in the crystals. The lower quality of the sample B resulted in a smaller Hall resistivity, which has in turn given a misleading phase shift in the case of Landau level indexing by the resistivity. This points to the necessity of using the conductivity oscillations instead of the resistivity for indexing, especially in the case when the Hall resistivity is not much higher than the transport resistivity. We also present unified indexing rules for constructing the Landau level diagrams for the quantum oscillations in conductivity, magnetic susceptibility, and magnetization based on the method commonly used in the topological insulators, i.e., where the integers are assigned to the minima in the conductivity. Besides indexing of minima and maxima of oscillations we also introduce indexing for the zeros, which increases the reliability of phase determination. The values of the Fermi wave vector, Fermi velocity, effective mass, and Dingle temperature have been extracted from the dHvA and the SdH oscillations.

[1] L. Fu, Phys. Rev. Lett. **106**, 106802 (2011).

[2] Y. Ando and L. Fu, Annu. Rev. Condens. Matter Phys. **6**, 361 (2015).

[3] T. Liang, Q. Gibson, J. Xiong, M. Hirschberger, S. P. Koduvayur, R. J. Cava, and N. P. Ong, Nat. Commun. **4**, 2696 (2013).

[4] Y. I. Ravich, B. A. Efimova, and I. A. Smirnov, *Semiconducting Lead Chalcogenides* (Plenum Press, New York, 1970).

[5] I. Zeljkovic, Y. Okada, M. Serbyn, R. Sankar, D. Walkup, W. Zhou, J. Liu, G. Chang, Y. J. Wang, M. Z. Hasan, F. Chou, H. Lin, A. Bansil, L. Fu, and V. Madhavan, Nat. Mater. **14**, 318 (2015).

[6] H. Li, H. He, H. Z. Lu, H. Zhang, H. Liu, R. Ma, Z. Fan, S. Q. Shen, and J. Wang, Nat. Commun. **7**, 10301 (2016).

[7] M. Neupane, S. Y. Xu, R. Sankar, N. Alidoust, G. Bian, C. Liu, I. Belopolski, T. R. Chang, H. T. Jeng, H. Lin, A. Bansil, F. Chou, and M. Z. Hasan, Nat. Commun. **5**, 3786 (2014).

[8] Z. K. Liu, B. Zhou, Y. Zhang, Z. J. Wang, H. M. Weng, D. Prabhakaran, S.-K. Mo, Z. X. Shen, Z. Fang, X. Dai, Z. Hussain, and Y. L. Chen, Science **343**, 864 (2014).

[9] S. Borisenko, Q. Gibson, D. Evtushinsky, V. Zabolotnyy, B. Büchner, and R. J. Cava, Phys. Rev. Lett. **113**, 027603 (2014).

[10] B.-J. Yang and N. Nagaosa, Nat. Commun. **5**, 4898 (2014).

[11] Q. D. Gibson, L. M. Schoop, L. Muechler, L. S. Xie, M. Hirschberger, N. P. Ong, R. Car, and R. J. Cava, Phys. Rev. B **91**, 205128 (2015).

[12] A. A. Burkov, M. D. Hook, and L. Balents, Phys. Rev. B **84**, 235126 (2011).

[13] S.-M. Huang, S.-Y. Xu, I. Belopolski, C.-C. Lee, G. Chang, B. Wang, N. Alidoust, G. Bian, M. Neupane, C. Zhang, S. Jia, A. Bansil, H. Lin, and M. Z. Hasan, Nat. Commun. **6**, 7373 (2015).

[14] A. A. Zyuzin and R. P. Tiwari, JETP Lett. **103**, 717 (2016).

[15] S.-Y. Xu, I. Belopolski, N. Alidoust, M. Neupane, C. Zhang, R. Sankar, S.-M. Huang, C.-C. Lee, G. Chang, B. K. Wang, G. Bian, H. Zheng, D. S. Sanchez, F. Chou, H. Lin, S. Jia, and M. Z. Hasan, Science **349**, 613 (2015).

[16] C. Zhang, S.-Y. Xu, I. Belopolski, Z. Yuan, Z. Lin, B. Tong, N. Alidoust, C.-C. Lee, S.-M. Huang, H. Lin, M. Neupane, D. S. Sanchez, H. Zheng, G. Bian, J. Wang, C. Zhang, T. Neupert, M. Z. Hasan, and S. Jia, Nat. Commun. **7**, 10735 (2016).

[17] H.-J. Kim, K.-S. Kim, J.-F. Wang, M. Sasaki, N. Satoh, A. Ohnishi, M. Kitaura, M. Yang, and L. Li, Phys. Rev. Lett. **111**, 246603 (2013).

[18] T. H. Hsieh, H. Lin, J. Liu, W. Duan, A. Bansil, and L. Fu, Nat. Commun. **3**, 982 (2012).

[19] Y. Tanaka, Z. Ren, T. Sato, K. Nakayama, S. Souma, T. Takahashi, K. Segawa, and Y. Ando, Nat. Phys. **8**, 800 (2012).

[20] S.-Y. Xu, C. Liu, N. Alidoust, M. Neupane, D. Qian, I. Belopolski, J. D. Denlinger, Y. J. Wang, H. Lin, L. A. Wray, G. Landolt, B. Slomski, J. H. Dil, A. Marcinkova, E. Morosan, Q. Gibson, R. Sankar, F. C. Chou, R. J. Cava, A. Bansil, and M. Z. Hasan, Nat. Commun. **3**, 1192 (2012).

[21] P. Dziawa, B. J. Kowalski, K. Dybko, R. Buczko, A. Szczerbakow, M. Szot, E. Lusakowska, T. Balasubramanian, B. M. Wojek, M. H. Berntsen, O. Tjernberg, and T. Story, Nat. Mater. **11**, 1023 (2012).

[22] C. M. Polley, P. Dziawa, A. Reszka, A. Szczerbakow, R. Minikayev, J. Z. Domagala, S. Safaei, P. Kacman, R. Buczko, J. Adell, M. H. Berntsen, B. M. Wojek, O. Tjernberg, B. J. Kowalski, T. Story, and T. Balasubramanian, Phys. Rev. B **89**, 075317 (2014).

[23] Y. Ando, J. Phys. Soc. Jpn. **82**, 102001 (2013).

[24] A. A. Taskin, F. Yang, S. Sasaki, K. Segawa, and Y. Ando, Phys. Rev. B **89**, 121302(R) (2014).

[25] M. Novak, S. Sasaki, K. Segawa, and Y. Ando, Phys. Rev. B **91**, 041203 (2015).

[26] J. C. W. Song, G. Refael, and P. A. Lee, Phys. Rev. B **92**, 180204(R) (2015).

[27] C. Shekhar *et al.*, Nat. Phys. **11**, 645 (2015).

[28] J. Feng, Y. Pang, D. Wu, Z. Wang, H. Weng, J. Li, X. Dai, Z. Fang, Y. Shi, and L. Lu, Phys. Rev. B **92**, 081306(R) (2015).

[29] J. Klier, I. V. Gornyi, and A. D. Mirlin, Phys. Rev. B **92**, 205113 (2015).

[30] C. Zhang, C. Guo, H. Lu, X. Zhang, Z. Yuan, Z. Lin, J. Wang, and S. Jia, Phys. Rev. B **92**, 041203(R) (2015).

[31] D. Shoenberg, *Magnetic Oscillations in Metals* (Cambridge University Press, Cambridge, 1984).

[32] H. Murakawa, M. S. Bahramy, M. Tokunaga, Y. Kohama, C. Bell, Y. Kaneko, N. Nagaosa, H. Y. Hwang, and Y. Tokura, Science **342**, 1490 (2013).

[33] $F = 8.5$ T, $m_c = 0.04 m_e$, $T_D = 2.8$ K, and $\phi_p = -0.36\pi$.

[34] H.-Z. Lu, J. Shi, and S.-Q. Shen, Phys. Rev. Lett. **107**, 076801 (2011).

[35] A. A. Taskin and Y. Ando, Phys. Rev. B **84**, 035301 (2011).

[36] D. Kim, S. Cho, N. P. Butch, P. Syers, K. Kirshenbaum, S. Adam, J. Paglione, and M. S. Fuhrer, Nat. Phys. **8**, 459 (2012).

[37] Z. K. Liu *et al.*, Nat. Mater. **13**, 677 (2014).